Perturbation theory for traveling droplets

L. M. Pismen
Department of Chemical Engineering and Minerva Center for Nonlinear Physics of Complex Systems, Technion-Israel Institute of Technology, 32000 Haifa, Israel
(Received 25 April 2006; published 24 October 2006)

The motion of chemically driven droplets is analyzed by applying a solvability condition of perturbed hydrodynamic equations affected by the adsorbate concentration. Conditions for traveling bifurcation analogous to a similar transition in activator-inhibitorsystems are obtained. It is shown that interaction of droplets leads to either scattering of mobile droplets or the formation of regular patterns, respectively, at low or high adsorbate diffusivity. The same method is applied to droplets running on growing terrace edges during surface freezing.

DOI: 10.1103/PhysRevE.74.041605 PACS number(s): 68.15.+e, 47.20.Ky, 68.43.−h

I. INTRODUCTION

Spontaneous motion of droplets on solid substrate driven by adsorption or chemical reactions that influence wetting properties has been observed in a number of experiments [1–4]. More recently, a reversible setup allowing for restoration of substrate properties has been realized experimentally [5,6]. This makes possible motion with self-intersecting trajectories lasting for extended periods of time. Spontaneous motion has been observed also in processes of surface freezing and melting [7]. The cause of chemically driven motion is deposition of a poorly wettable material on the substrate or, alternatively, dissolution of an adsorbed wettable layer beneath the droplet. As a result, the droplet tends to migrate to the area with more favorable wetting properties outside its footprint. The direction of motion, originally chosen at random, is sustained because the area left behind is either permanently left nonwettable or takes time being restored. Chemically driven motion is of interest both in microfluidics applications and as a possible mechanism for the formation of surface patterns.

The theoretical model of chemically driven droplet motion presented recently [8,9] combined hydrodynamic equations in lubrication approximation with a linear reaction-diffusion equation for an adsorbed species. The model included a precursor layer that served to resolve the contact line singularity. The model equations were solved numerically, mapping the regimes of motion and their dependence on various parameters of the problem. The results showed, in particular, that droplets become immobile when diffusion and substrate modification are sufficiently fast. The theory relied, however, on the presence of a macroscopic precursor layer, which is unlikely to be formed under experimental conditions of Refs. [5,6]. Moreover, the computations were restricted to moderate ratios of the bulk droplet size to the precursor layer thickness, since numerical routines are all but impossible to implement for realistic ratios of many orders of magnitude.

In this paper, I present an analytical solution of the problem combining an integral solution of the reaction-diffusion equation for a steadily propagating droplet [10] with velocity computation using a solvability condition of perturbed hydrodynamic equations. The perturbation method applied to the hydrodynamic problem is described in Sec. II. The general approach, based on the lubrication approximation, is the same as in the theory of creeping motion of droplets under the action of externally imposed gradients. The perturbation approach to the problem of motion driven by surface inhomogeneities was pioneered by Greenspan [11] who had, however, to rely on a phenomenological relation for the motion of the contact line. Brochard [12] derived droplet translation velocity using integral balances between various driving forces and viscous dissipation. The latter poses a special problem in view of the notorious contact line singularity, which can be resolved either by introducing a slip length [13,14] or by allowing for an ultrathin precursor layer [15,16]. The latter approach has been applied to derive integral conditions for a droplet driven either by an external field (gravity) or by changes in the precursor thickness due to droplet interactions [17]. The result, applied later also to two-dimensional (2D) droplets driven by a difference of advancing and receding contact angles [18], turned out to give even better approximation than more elaborate theory using a precise solution of lubrication equations to compute the shape of the bulk droplet.

The integral condition for droplet motion will be derived in Sec. II B in a more formal way as a solvability condition of perturbation equations, using an eigenfunction of the adjoint problem introduced earlier for a 2D problem [19]. The contact line singularity will be resolved, however, in Sec. II C in a more traditional way through introducing a slip length, and the solvability condition will be rederived for this model. Both ways of eliminating the singularity are indistinguishable on a macroscopic level, leading to a model-dependent logarithmic factor [20], and therefore the result does not need to rest on the existence of a macroscopic precursor or depend on a precise way the hydrodynamic equations have to be modified in the immediate vicinity of the substrate. Since the presence of a precursor layer in the experiment of Refs. [5,6] is an unlikely conjecture, and introducing it would require making special assumptions on the surfactant transport in this layer, resolving the contact line singularity through effective slip appears to be natural in this case.

In Secs. III and IV, I shall concentrate on the reversible setup of Refs. [5,6]. The surfactant transport and adsorption/desorption model follows closely that of Refs. [8,9]. The process, in accordance with the experimental setup, is viewed as quasistationary, so that the bulk surfactant concentrations in both the droplet and the embedding phase remain

constant on the characteristic time scale of droplet motion. The surfactant adsorption and desorption rate and, as a result, the droplet propagation speed change slowly with time, as the droplet is gradually saturated by the surfactant, and the motion eventually ceases as equilibrium is reached. The hydrodynamic parameters, such as surface tension and slip length, may change in the course of the process as well, but the relations derived in the quasistationary approximation apply at any moment of time, as the changes are slow.

The basic approach is described in Sec. III A, followed by the velocity computation for a single steadily propagating droplet both in fast (Sec. III B) and slow (Sec. III C) diffusion limits and in a general case (Sec. III D). The principal result obtained in the fast diffusion (slow velocity) limit is the existence of a supercritical traveling bifurcation analogous to a similar transition in activator-inhibitor systems [21,22]. I further investigate droplet interactions on either side of this transition, resulting in relaxation to a regular stationary pattern sustained by long-range repulsion (Sec. IV A) or scattering of mobile droplets (Sec. IV B). The problem of motion driven by surface freezing or melting is briefly considered in Sec. V.

II. PERTURBATION ANALYSIS

A. Basic equations

The droplet shape is described in the lubrication approximation by the thin film equation

$$h_t = -\frac{\gamma}{\eta}\boldsymbol{\nabla}\cdot[q(h)\,\boldsymbol{\nabla}\nabla^2 h]. \tag{1}$$

Here gravity and other external forces are neglected, γ is the surface tension of the droplet interface, and $\boldsymbol{\nabla}$ is the 2D gradient operator in the plane of the substrate. The simplest suitable expression for the effective mobility function $q(h)$, obtained assuming the viscosity η of the droplet to be much larger than that of the surrounding fluid and applying the Navier slip boundary condition, is

$$q(h) = \frac{h^2}{3}(h+3\lambda), \tag{2}$$

where λ is the slip length.

The boundary condition on the droplet contour Γ, i.e., the contact line, is $\boldsymbol{n}\cdot\boldsymbol{\nabla}h=-\theta$, where $\boldsymbol{n}$ is the outer normal to Γ and θ is the contact angle. The droplet is stationary and has a circular footprint $\mathcal{R}$ with a radius R when the equilibrium contact angle does not depend on position explicitly. Variations of the contact angle caused by the substrate modification, generally, distort the droplet shape. We shall assume that deviations from a reference constant value θ_0 are weak, so that the contact angle can be presented as $\theta=\theta_0+\epsilon\tilde{\theta}$, where ϵ is the bookkeeping small parameter. Respectively, the deviation of the droplet profile from the stationary circularly symmetric shape $h_0(r)$ is $\tilde{h}(r,\phi)$, where r,ϕ are polar coordinates.

Both $\tilde{h}$ and $\tilde{\theta}=-(\partial\tilde{h}/\partial r)_\Gamma$ can be expanded in a Fourier series

$$\tilde{h}(r,\phi)=\sum h_n(r)e^{in\phi}, \quad \tilde{\theta}(\phi)=\sum \theta_n e^{in\phi}. \tag{3}$$

All harmonic perturbations with $n>1$ distort the circular shape of the droplet footprint (hence of the contact line Γ) and can be accommodated by a stationary droplet with the respective symmetry. The first harmonic (dipole $n=1$) is, however, an exception, since the respective perturbation of Γ is equivalent to translation without change of form. Therefore the dipole component of $\tilde{\theta}$ is expected to set the droplet into slow motion with a velocity $\epsilon\boldsymbol{U}\ll 1$, without affecting the shape of its footprint (to the first order in ϵ).

We shall be looking for a solution of Eq. (1) defining a droplet moving with a constant speed without change of form. The time dependence in Eq. (1) is reduced then to translation with a velocity $\epsilon\boldsymbol{U}$, as yet unknown, leading to a quasistationary equation in the comoving frame

$$-(\epsilon\eta/\gamma)\boldsymbol{U}\cdot\boldsymbol{\nabla}h+\boldsymbol{\nabla}\cdot[q(h)\,\boldsymbol{\nabla}\nabla^2 h]=0. \tag{4}$$

The zero order function is the stationary solution which satisfies the constant curvature condition $\boldsymbol{\nabla}^2 h_0=\text{const}$. The solution with a fixed contact angle θ_0 is just a paraboloidal cap

$$h_0(r)=\frac{R\theta_0}{2}\left[1-\left(\frac{r}{R}\right)^2\right], \tag{5}$$

where R is the droplet radius. The perturbed shape of the moving droplet can be obtained to $O(\epsilon)$ by expanding the linearized Eq. (4) in a Fourier series. It turns out, however, that a relation between the velocity and the contact angle distortion can be obtained without actually solving this equation; it is sufficient to compute its *solvability condition*.

B. Translational solvability condition

The linearized Eq. (4) has a general form

$$\mathcal{L}\tilde{h}+\Psi(\boldsymbol{x})=0, \tag{6}$$

which contains the linear operator

$$\mathcal{L}\tilde{h}\equiv\boldsymbol{\nabla}\cdot[q(h_0)\,\boldsymbol{\nabla}\nabla^2\tilde{h}] \tag{7}$$

and the inhomogeneity

$$\Psi(\boldsymbol{x})=-(\eta/\gamma)\boldsymbol{U}\cdot\boldsymbol{\nabla}h_0. \tag{8}$$

The operator $\mathcal{L}$ is not self-adjoint. The adjoint equation defining the translational Goldstone mode φ is

$$\mathcal{L}^\dagger\varphi\equiv\nabla^2\boldsymbol{\nabla}\cdot[q(h_0)\,\boldsymbol{\nabla}\varphi]=0. \tag{9}$$

This equation is satisfied by the eigenfunction defined through its gradient as

$$\boldsymbol{\nabla}\varphi=\boldsymbol{I}\frac{h_0}{q(h_0)}, \tag{10}$$

where $\boldsymbol{I}$ is an arbitrarily directed unit vector. Taking two vectors $\boldsymbol{I}$ along the two Cartesian axes gives two Goldstone modes corresponding to two translational degrees of freedom in the plane. We shall not need an explicit integral form of φ,

which can be obtained by solving Eq. (10) and depends on appropriate boundary conditions.

The solvability condition of Eq. (6) is obtained by multiplying it by φ and integrating over the unperturbed droplet footprint area $\mathcal{R}$. In an unbounded region, this would be equivalent to the orthogonality of the inhomogeneity $\Psi(\boldsymbol{x})$ to the Goldstone mode $\varphi(\boldsymbol{x})$. Since, however, the region $\mathcal{R}$ is bounded by a contour Γ, the solvability condition depends on the boundary conditions on Γ and includes both area and contour integrals.

The eigenfunction φ has the symmetry of a dipole oriented along $\boldsymbol{I}$. The inhomogeneity is likewise a dipole oriented along $\boldsymbol{U}$. Therefore $\boldsymbol{I}$ can be directed along the propagation direction, and the area integral can be presented after integrating by parts as

$$\int_{\mathcal{R}} \varphi(\boldsymbol{x})\Psi(\boldsymbol{x})d\boldsymbol{x} = \frac{\eta U}{\gamma}\int_{\mathcal{R}} \frac{h_0^2}{q(h_0)}d\boldsymbol{x} \equiv \frac{\eta U}{\gamma}\mathcal{J}, \tag{11}$$

where $U=|\boldsymbol{U}|$. The integral $\mathcal{J}$ is interpreted as the *friction factor*.

A contour integral dependent on the unknown first-order function $\tilde{h}$ is contributed by the operator $\mathcal{L}$ when it is multiplied by φ and integrated by parts:

$$\mathcal{I}_\Gamma = \oint_\Gamma \varphi(s)q(h_0)\boldsymbol{n}\cdot\boldsymbol{\nabla}\nabla^2\tilde{h}ds - \oint_\Gamma (\boldsymbol{n}\cdot\boldsymbol{I})h_0\nabla^2\tilde{h}ds + \oint_\Gamma (\boldsymbol{I}\cdot\boldsymbol{\nabla}h_0)\boldsymbol{n}\cdot\boldsymbol{\nabla}\tilde{h}ds - \oint_\Gamma (\boldsymbol{n}\cdot\boldsymbol{I})\nabla^2 h_0\tilde{h}ds. \tag{12}$$

The first integral vanishes, since at $h_0\to 0$ $q(h_0)\propto h_0^2$, while φ, as follows from Eq. (10), is only logarithmically divergent. The second integral vanishes at $h_0(\Gamma)=0$ as well. The third integral expresses the *boundary force* due to the variable part of the contact angle $\tilde{\theta}=\theta-\theta_0=-\epsilon^{-1}\boldsymbol{n}\cdot\boldsymbol{\nabla}\tilde{h}$. The last integral depends on droplet shape distortion when $\tilde{h}(\Gamma)\neq 0$.

C. Computation of the propagation speed

The translation speed is determined by the dipole component of the Fourier expansion. Since $\boldsymbol{n}\cdot\boldsymbol{I}=\cos\phi$ (where the polar angle ϕ is counted from the direction of motion) and $\nabla^2 h_0=\text{const}$, the last integral in Eq. (12) is proportional to the dipole component $h_1(\Gamma)$ of $\tilde{h}(\Gamma)$. We have noticed that this component does not affect the shape of the droplet footprint, besides its displacement. One has to require therefore $h_1(\Gamma)=0$; hence this integral vanishes. The remaining boundary force integral is evaluated using the identity $\boldsymbol{I}\cdot\boldsymbol{\nabla}h_0=-\theta_0\cos\phi$ as

$$\mathcal{I}_\Gamma = -\theta_0 R\int_{-\pi}^{\pi}\cos\phi\tilde{\theta}(\phi)d\phi = -\theta_0 R\,\mathrm{Re}\,\theta_1 \equiv -\mathcal{F}. \tag{13}$$

The friction factor $\mathcal{J}$ diverges at $\lambda=0$, which is the reason for introducing the slip length in Eq. (2). Since, however, this length is very small, being measured on a molecular scale, the integral can be evaluated by separating it into two parts. Near the contact line, i.e., in a ring $R\leqslant r\leqslant R-l$ where $\lambda\ll l\ll R$, the integration can be carried out using the linearized profile $h_0=\theta_0(R-r)$. This yields, asymptotically at $l\gg\lambda$,

$$\mathcal{J}_1 = 6\pi R\int_{R-l}^{R}[\theta_0(R-r)+3\lambda]^{-1}dr \asymp \frac{6\pi R}{\theta_0}\ln\frac{\theta_0 l}{3\lambda}. \tag{14}$$

In the bulk region $r\leqslant R-l$, λ can be neglected, and the integration yields, asymptotically at $l\ll R$,

$$\mathcal{J}_2 = \frac{6\pi}{R\theta_0}\int_0^{R-l}\left[1-\left(\frac{r}{R}\right)^2\right]^{-1}rdr \asymp \frac{6\pi R}{\theta_0}\ln\frac{R}{2l}. \tag{15}$$

When both integrals add up, the auxiliary length l falls out, resulting in an expression containing the logarithm of the ratio of the macroscopic and microscopic scales:

$$\mathcal{J} = \frac{6\pi R}{\theta_0}\ln\frac{\theta_0 R}{6\lambda}. \tag{16}$$

Thus the dipole component of the solvability condition defining the droplet velocity reads

$$U = \frac{\gamma}{\eta}\frac{\mathcal{F}}{\mathcal{J}} = \frac{\gamma\theta_0^2}{6\pi\eta}\ln^{-1}\frac{\theta_0 R}{6\lambda}\int_{-\pi}^{\pi}\cos\phi\tilde{\theta}(\phi)d\phi. \tag{17}$$

III. CHEMICAL SELF-PROPULSION

A. Substrate modification

Variation of the contact angle is caused by substrate modification, e.g., dissolution of the surfactant adsorbed on the substrate in experiments of Sumino *et al.* [5,6]. The surfactant adsorption and desorption is described by a linear kinetic equation $dc/dt=k_a c_0-kc$, where c_0 is the bulk concentration and k_a, k are kinetic constants; the latter is assumed for simplicity to be the same in the droplet and the continuous phase. Taking into account surface diffusion and assuming the bulk concentration in the droplet to be negligible, we write the adsorption-diffusion equation for the surfactant coverage on the substrate in the dimensionless form

$$c_t = \nabla^2 c - c + H(\boldsymbol{x}), \tag{18}$$

where $H(\boldsymbol{x})$ equals 1 outside and 0 inside the droplet footprint. The surfactant coverage c is scaled by the coverage in equilibrium with the surfactant concentration in the continuous phase $k_a c_0/k$, time by the inverse desorption rate constant k, and length by $\sqrt{D/k}$, where D is the surfactant diffusivity on the substrate. At later stages of the process when surfactant accumulates in the droplet bulk, one can use the same equation, taking into account that only the difference of adsorption rates outside and inside the droplet is important, and replacing $k_a c_0$ by the difference of the respective values.

The characteristic velocity scale is $U^*=\sqrt{Dk}$. If Eq. (4) is brought to a dimensionless form by replacing $\epsilon U=U^* v$, the advective term is recast as $\mathrm{Ca}\, v\cdot\boldsymbol{\Delta}h$, where $\mathrm{Ca}=\sqrt{Dk}\eta/\gamma$ is the capillary number based on the characteristic "chemical" velocity U^*, or the ratio of the "chemical" velocity to the characteristic "hydrodynamic" velocity γ/η,

which determines the influence of viscous stresses on the droplet shape sustained by surface tension. This implies that the capillary number is the true small parameter of the problem; deviations of the contact angle should be of $O(\mathrm{Ca})$ to justify the perturbation approach. This condition is likely to hold under realistic experimental conditions, since surface diffusion is slow, which insures that the shape of chemically propelled droplets is only weakly distorted by viscous stresses.

Equation (18) transformed to the frame moving with a dimensionless velocity v along the x axis is

$$vc_x + \nabla^2 c - c + H(\boldsymbol{x}) = 0. \tag{19}$$

The solution of this equation can be expressed with the help of an appropriate Green's function through an integral over the droplet footprint area and subsequently transformed into a contour integral with the help of the Gauss theorem [10]. For a circular contour with a dimensionless radius (Thiele modulus) $a=R\sqrt{k/D}$, the concentration on its boundary, which determines the propagation speed, is computed in this way as

$$\begin{aligned} c(\phi) = 1 - \frac{a}{2\pi}\int_{-\pi}^{\pi} e^{-1/2va(\cos\phi - \cos\xi)} \\ \times\left[\frac{v}{2}\cos\xi K_0\left(2a\sqrt{1+\frac{v^2}{4}}\sin\frac{|\phi-\xi|}{2}\right)\right. \\ + \sqrt{1+\frac{v^2}{4}}\sin\frac{|\phi-\xi|}{2} \\ \left.\times K_1\left(2a\sqrt{1+\frac{v^2}{4}}\sin\frac{|\phi-\xi|}{2}\right)\right]d\xi, \end{aligned} \tag{20}$$

where K_n (and I_n below) are modified Bessel functions.

Assuming the contact angle to be a linear function of the surfactant coverage, $\epsilon\tilde{\theta}=-\beta c$, the propagation velocity is computed by solving the equation obtained by combining Eqs. (17) and (20):

$$v = \frac{M}{\pi}\int_0^{\pi} \tilde{c}(\phi;v)\cos\phi\, d\phi, \tag{21}$$

where $\tilde{c}=1-c$ and all relevant parameters, except the dimensionless droplet radius a in Eq. (20), are lumped into a single dimensionless combination, which can be called the *droplet mobility* parameter:

$$M = \frac{\theta_0^2\gamma\beta}{6\eta\sqrt{Dk}}\ln^{-1}\frac{\theta_0 R}{6\lambda}. \tag{22}$$

The parameter M retains a weak logarithmic dependence on the droplet radius.

B. Traveling bifurcation

Simplified expressions can be obtained in the limiting cases $v \ll 1$ and $v \gg 1$. The perturbation approach is still applicable also in the latter case, since the capillary number is typically very small.

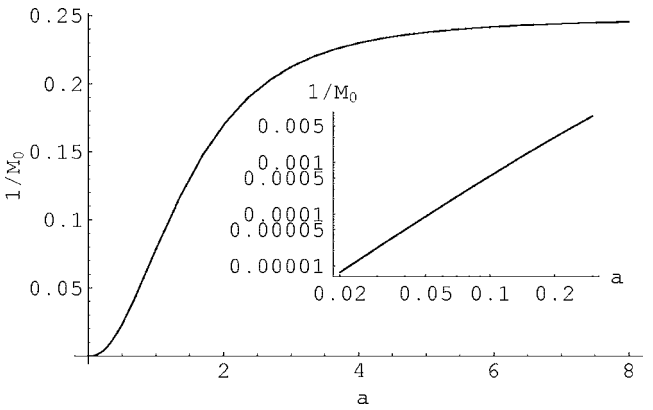

FIG. 1. The critical value M_0^{-1} as a function of the dimensionless droplet radius a. Inset: blowup near the origin on logarithmic scale. The droplets are mobile below this curve.

The limit $v \ll 1$ (i.e., fast diffusion) is analogous to the fast inhibitor limit in reaction-diffusion systems, which is conducive to formation of stationary patterns [22]. Equation (20) is expanded in this limit to the first order in v as

$$\begin{aligned} \tilde{c}(\phi) = \frac{a}{\pi}\int_0^{\pi}\left\{\sin\frac{\zeta}{2}K_1\left(2a\sin\frac{\zeta}{2}\right)\right. \\ + v\cos\phi\left[\frac{1}{2}\cos\zeta\, K_0\left(2a\sin\frac{\zeta}{2}\right)\right. \\ \left.\left. + a\sin^3\frac{\zeta}{2}\,K_1\left(2a\sin\frac{\zeta}{2}\right)\right] + O(v^2)\right\}d\zeta, \end{aligned} \tag{23}$$

where $\zeta=\xi-\phi$. In the leading $O(1)$ order, the surfactant distribution is circularly symmetric. The first-order dipole term in Eq. (23) is the only one contributing to the integral in Eq. (21) (another term vanishing upon integration is omitted). The angular integrals are evaluated using the identities

$$\Phi_k(a) = \int_0^{\pi}\sin^{2k}\frac{\phi}{2}K_0\left(2a\sin\frac{\phi}{2}\right)d\phi = -\frac{1}{2a}\frac{d(a\Psi_{k-1})}{da},$$

$$\Psi_k(a) = \int_0^{\pi}\sin^{2k+1}\frac{\phi}{2}K_1\left(2a\sin\frac{\phi}{2}\right)d\phi = -\frac{1}{2}\frac{d\Phi_k}{da},$$

starting from $\Phi_0(a)=\pi I_0(a)K_0(a)$. Plugging the resulting expressions in Eq. (21) yields the condition for the onset of motion

$$M_0^{-1} = \frac{a^2}{2}[I_1(a)K_2(a) - I_0(a)K_1(a)]. \tag{24}$$

The critical value M_0^{-1} as a function of a is plotted in Fig. 1. Since the radial dependence in Eq. (24) saturates when the droplet radius far exceeds the diffusional range, so that $M_0 \to 4$ at $a\to\infty$, no droplet can move below this limiting value.

Because of the logarithmic dependence of M on the droplet radius, the size dependence of the traveling threshold in Eq. (24) still remains implicit. An explicit dependence can be extracted after rewriting Eq. (22) as

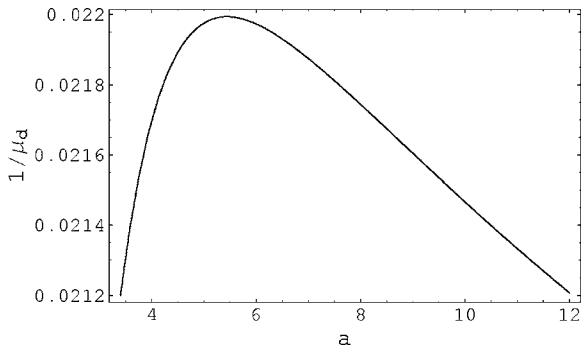

FIG. 2. The critical value of μ_d^{-1} as a function of the dimensionless droplet radius a for $\lambda_d=10^{-4}$.

$$M=\mu_d \ln^{-1}\frac{a}{\lambda_d},\quad \mu_d=\frac{\theta_0^2\gamma\beta}{6\eta\sqrt{Dk}},\quad \lambda_d=\frac{6\lambda}{\theta_0}\sqrt{\frac{k}{D}}. \tag{25}$$

In the limit $a\gg 1$ when the critical value M_0 in Eq. (24) approaches the limit $M_0=4$, the droplet is mobile at $a<\lambda_d \exp(\mu_d/4)$. This suggests that the radius of mobile droplets is bounded both from below and above, as it indeed follows from the existence of a maximum in the radial dependence of the critical value of the parameter μ_d, such as seen in Fig. 2.

Beyond the critical point, the velocity can be obtained using further terms in the expansion (23). The dipole component of the term quadratic in v vanishes, and therefore there is no contribution to motion in this order. The dipole component of the third-order term is $\alpha_3 v^3$ where

$$\alpha_3=-\frac{a^3}{16}[I_0(a)K_1(a)-I_1(a)K_0(a)-a^{-1}I_1(a)K_1(a)]. \tag{26}$$

This coefficient is negative; hence the bifurcation is supercritical and propagation is possible at $M>M_0$. For small deviations $M_2=M-M_0>0$, the velocity is $v=\sqrt{-M_2/\alpha_3}$.

C. Nondiffusive limit

In the opposite limit when diffusion is negligible, the diffusional scaling of the droplet radius and velocity becomes invalid, and dimensionless relations should be constructed using the capillary number $\mathrm{Ca}=U\eta/\gamma$ and the rescaled dimensionless radius $\rho=Rk\eta/\gamma$. The surfactant concentration can be obtained directly by integrating along the direction of motion with the initial condition $c=1$ on the advancing contact line ($|\phi|<\pi/2$). The resulting concentration on the receding contact line,

$$c(\phi)=e^{-2\tau\cos\phi}, \tag{27}$$

depends only on the ratio

$$\tau=\frac{a}{v}=\frac{kR}{U}=\frac{\rho}{\mathrm{Ca}}. \tag{28}$$

The equation for τ following from Eq. (17) is

$$P=\frac{\tau}{\pi}\int_0^{\pi/2}\cos\phi(1-e^{-2\tau\cos\phi})d\phi\equiv\tau F(\tau), \tag{29}$$

containing a single parameter

$$P=\frac{a}{M}=\frac{6\eta Rk}{\theta_0^2\gamma\beta}\ln\frac{\theta_0 R}{6\lambda}=\frac{\rho}{\mu_h}\ln\frac{\rho}{\lambda_h}, \tag{30}$$

where $\mu_h=\frac{1}{6}\beta\theta_0^2$, $\lambda_h=6\lambda\gamma/(k\eta\theta_0)$. The function $F(\tau)$ is evaluated as

$$F(\tau)=\frac{1}{\pi}+\frac{1}{2}[I_1(2\tau)-\mathbf{L}_{-1}(2\tau)], \tag{31}$$

where $\mathbf{L}_n(x)$ is a Struve function. The function $F(\tau)$ increases monotonically from 0 at $\tau=0$ to $1/\pi$ at $\tau\to\infty$.

The dependence of the capillary number on the dimensionless droplet radius can be obtained analytically in two limiting cases corresponding to the unsaturated and saturated regimes, respectively, at small and large τ. In the former case, one can use the approximation $F(\tau)=\tau/2+O(\tau^2)$ to obtain

$$\mathrm{Ca}\approx\left[\frac{\rho\mu_h}{2\ln(\rho/\lambda_h)}\right]^{1/2}. \tag{32}$$

In the opposite limit $\tau\gg 1$, $F(\tau)\approx 1/\pi$ and

$$\frac{1}{\mathrm{Ca}}\approx\frac{\pi}{\mu_h}\ln\frac{\rho}{\lambda_h}. \tag{33}$$

Thus the velocity increases with droplet size in the unsaturated and decreases in the saturated regime, in agreement with experiment [3] and earlier computations [9]. For intermediate values of τ, the dependence of velocity on radius obtained by solving Eq. (29) numerically is plotted in Fig. 3.

D. General case

In a general case, Eq. (21) can be rewritten as $M^{-1}=G(a,v)$ and solved after computing numerically the double integral

$$G(a,v)=\frac{a}{\pi^2 v}\int_0^{\pi}\cos\phi d\phi\int_{-\pi}^{\pi}e^{-1/2va[\cos\phi-\cos(\phi+\zeta)]}\times\left[\frac{v}{2}\cos(\phi+\zeta)K_0\left(2a\sqrt{1+\frac{v^2}{4}}\sin\frac{|\zeta|}{2}\right)+\sqrt{1+\frac{v^2}{4}}\sin\frac{|\zeta|}{2}K_1\left(2a\sqrt{1+\frac{v^2}{4}}\sin\frac{|\zeta|}{2}\right)\right]d\zeta. \tag{34}$$

The function $G(a,v)$ is plotted against v at several values of a in Fig. 4. The curves peak at the ordinate axis at the bifurcation value M_0^{-1} given by Eq. (24).

IV. DROPLET INTERACTIONS

A. Relaxation to a stationary pattern

At high diffusivities when droplets do not travel spontaneously, they still can move under the influence of mutual

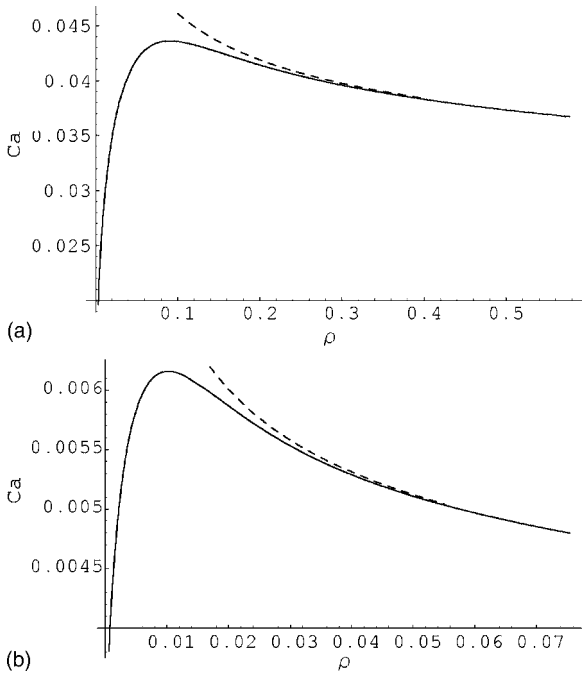

FIG. 3. The dependence of the capillary number Ca on the dimensionless radius ρ for $\lambda_h=10^{-4}$ and $\mu_h=1$ (a) and $\mu_h=0.1$ (b). The dashed line shows the asymptotic dependence (33).

interactions. The surfactant depletion in the far field of a stationary droplet (at distances far exceeding its radius) is well-approximated by the stationary solution of Eq. (18) with c replaced by $\tilde{c}$ and $H(\boldsymbol{x})$ by the delta-function multiplied by the droplet area:

$$\tilde{c} = \frac{1}{2}a^2 K_0(r). \tag{35}$$

The circular symmetry of the surfactant distribution around a single droplet is perturbed by the far field of its neighbors. The resulting repelling interaction induces, according to Eq. (17), motion with the velocity proportional to the concentration gradient at the droplet location. If there is a number of droplets, their action is additive. This leads to the equation of motion for droplet centers $\boldsymbol{X}_j$

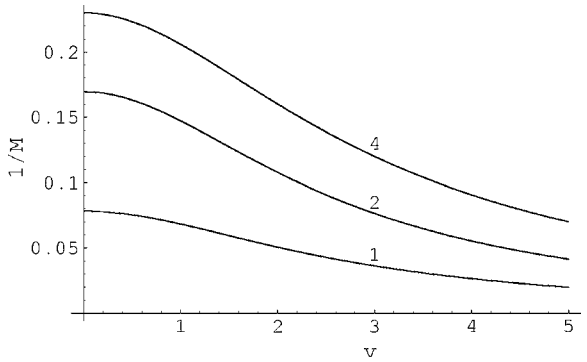

FIG. 4. Plots of $G(a,v)$ defined by Eq. (34) as a function of v; the values of a are marked at the respective curves.

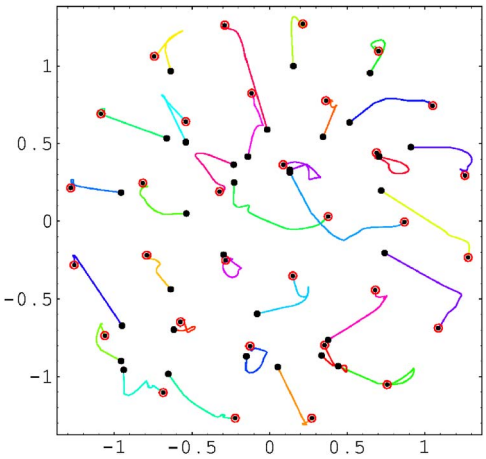

FIG. 5. (Color online) Trajectories of identical droplets moving according to Eq. (36) with added centripetal force. The dots mark the original random arrangement, and the circles, final positions.

$$\frac{d\boldsymbol{X}_j}{dt} = M_j a_j \sum_{k\neq j} \frac{\boldsymbol{X}_j - \boldsymbol{X}_k}{|\boldsymbol{X}_j - \boldsymbol{X}_k|} \frac{a_k^2}{2} K_1(|\boldsymbol{X}_j - \boldsymbol{X}_k|). \tag{36}$$

This is a gradient dynamical system

$$\frac{d\boldsymbol{X}_j}{dt} = -\frac{M_j}{a_j}\frac{\partial V}{\partial \boldsymbol{X}_j}, \tag{37}$$

evolving to minimize the potential

$$V = \frac{1}{2}\sum_{k\neq j} a_j^2 a_k^2 K_0(|\boldsymbol{X}_j - \boldsymbol{X}_k|). \tag{38}$$

In a "thermodynamic" limit of an infinitely large region containing an infinite number of droplets, the potential is expected to be minimized by a regular hexagonal pattern with spacing dependent on the number density of droplets. The ordering tendency is demonstrated by an example of evolution shown in Fig. 5. For numerical convenience, the confinement is effected in this computation by adding to Eq. (38) a centripetal external potential $V_0 = m\Sigma|\boldsymbol{X}_j|^2$ with a suitable constant m. One can see that evolution starting from a random arrangement of droplets evolves to a regular pattern where circles mark final positions falling roughly on a hexagonal grid. This might be a practical way to arrange a regular dewetting pattern on a homogeneous substrate.

B. Scattering

The surfactant depletion in the far field of a steadily moving droplet can be obtained by solving Eq. (19) with c replaced by $\tilde{c}$ and $H(\boldsymbol{x})$ by the delta-function multiplied by the droplet area. The solution is expressed in polar coordinates r, ϕ centered on the droplet as

$$\tilde{c} = \frac{a^2}{2} e^{-1/2vr\cos\phi} K_0\left(r\sqrt{1+\frac{v^2}{4}}\right). \tag{39}$$

The depletion field is strongly asymmetric, with a slower decay behind the droplet (Fig. 6).

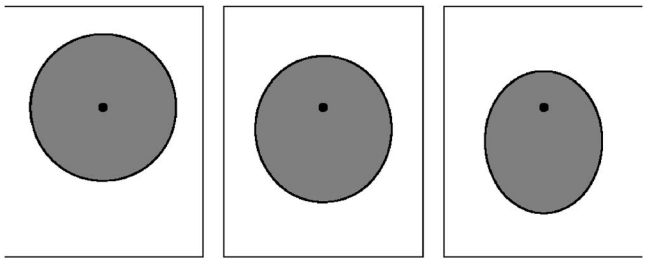

FIG. 6. Surfactant depletion in the far field of a stationary droplet (left) and droplets propagating with the speed $v=1$ (center) and $v=2$ (right). The droplet position is marked by a dot. The area with surfactant depletion above the same level is shaded, showing the depletion in the tail region increasing at higher speed.

Droplets moving one toward another are scattered by mutually repelling interaction created by the gradient of the far field. The problem remains tractable in the quasistationary approximation as long as velocity induced by interaction is much smaller than the speed of self-propelled motion. Otherwise, the far field becomes dependent on the entire history of motion, and solving the full nonstationary problem (18) is necessary.

Consider as an example two droplets of equal size propagating along the x axis with identical speed v on antiparallel trajectories shifted by the interval $2Y$, as in Fig. 7. Since a deflected droplet keeps moving on a perturbed course, the scattering action is equivalent to acceleration in the direction normal to self-propelled motion. Restricting to the quasistationary approximation, the dynamic equation for the deviation $\tilde{y}$ normal to the original trajectory is therefore

$$\frac{d^2\tilde{y}}{dt^2} = -Ma\frac{\partial \tilde{c}}{\partial y}, \tag{40}$$

where the derivative of the surfactant depletion given by Eq. (39) is computed at a current distance between the droplets at the moment t equal to

$$r(t) = 2[(vt)^2 + (Y+\tilde{y})^2]^{1/2}, \tag{41}$$

where the moment of closest approach is taken as $t=0$. Neglecting the change of the velocity component along the x-axis, time t in Eq. (40) can be replaced by x/v. A typical trajectory obtained by integration is shown in Fig. 7 and a more quantitative example of the change of the scattering angle with distance is shown in Fig. 8. Take note that, due to a faster decay of depletion ahead of the droplet, scattering largely accumulates already after the droplets have passed the point of closest approach.

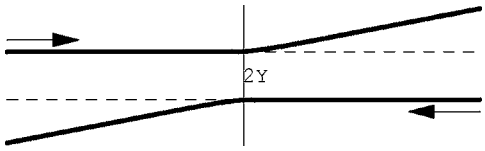

FIG. 7. Scattering trajectories. The vertical line marks the location of the closest approach.

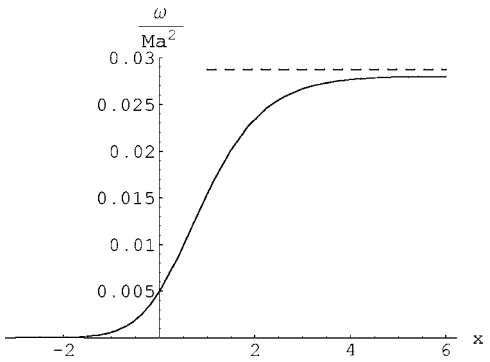

FIG. 8. The change of the scattering angle with distance for $v=1$, $Y=2$. The dashed line shows the scattering angle at infinity computed with the help of Eq. (42).

For moderate deviations, a reasonable approximation for the scattering angle at infinity $\omega=\tilde{y}'(\infty)$ gives the formula neglecting $\tilde{y}$ compared to Y:

$$\omega = \frac{MYa^3}{2v}\sqrt{1+\frac{v^2}{4}}\int_{-\infty}^{\infty}\frac{e^{vx}}{\sqrt{x^2+Y^2}}K_1(r\sqrt{(4+v^2)(x^2+Y^2)})dx. \tag{42}$$

Scattering angle computed with the help of this formula only weakly depends on velocity [Fig. 9(a)]. A much stronger dependence on the separation interval is shown in logarithmic coordinates in Fig. 9(b).

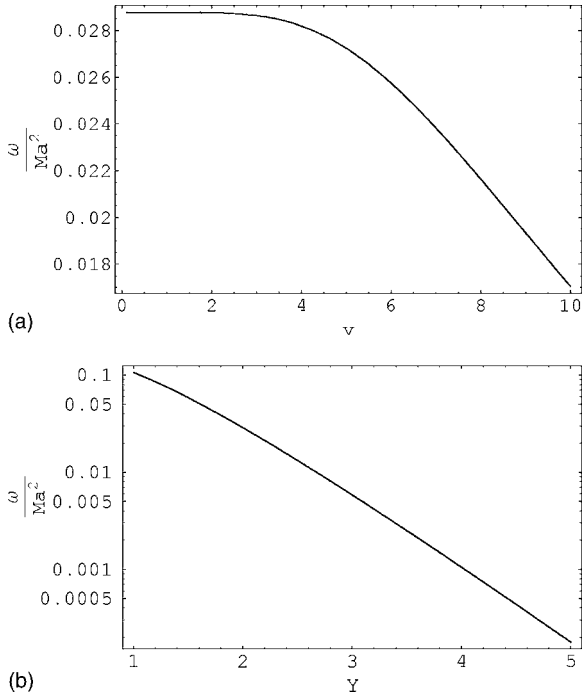

FIG. 9. Dependence of the change of the scattering angle on velocity for $Y=2$ (a) and its dependence on the separation interval for $v=1$ (b). Both curves are computed using Eq. (42).

V. SURFACE FREEZING AND MELTING

A different mechanism of spontaneous motion has been observed in processes of surface freezing and melting [7]. In these experiments, liquid alkane wets silicon substrate better than a frozen smectic layer. Respectively, the equilibrium contact angle increases with growing thickness of smectic, and a droplet tends to slip to a lower level when placed at a terrace edge.

For a droplet sitting on a terrace as shown in Fig. 10(a), $\tilde{\theta}$ has distinct constant values on segments $|\phi|<\psi$ and $\psi<|\phi|<\pi$. The contact angle is smaller at the lower terrace, which we place on the right; we take this value as θ_0 and denote the contact angle at the higher terrace as $\theta_0+\tilde{\theta}$. Then the velocity defined by Eq. (17) is

$$U = U_0 \sin\psi, \quad U_0 = \tilde{\theta}\frac{\gamma}{\eta}\frac{\theta_0^2}{6\pi}\ln^{-1}\frac{\theta_0 R}{6\lambda}. \tag{43}$$

During freezing, the change of the angular front position ψ due to propagation of the freezing front beneath the droplet with a constant velocity C obeys $R\sin\psi\, d\psi = -C dt$. Due to the droplet motion, the net front velocity relative to the droplet center is $C-U$. Thus the dynamic equation of the angular position is

$$R\frac{d\psi}{dt} = U_0 - \frac{C}{\sin\psi}. \tag{44}$$

The stationary position is $\psi_0=\arcsin(C/U_0)$; U_0 is the maximum speed allowing for this equilibrium. The configuration is stable at $\cos\psi<0$, i.e., $\psi>\pi/2$, which can be readily seen by linearizing Eq. (44) near $\psi=\psi_0$. Under this condition, the length of the segment where the contact angles on the advancing and receding sides are different decreases when the droplet slides ahead, so that the freezing front catches up and the stationary configuration is restored. Another equilibrium position at $\psi<\pi/2$ is unstable. This is in agreement with the disposition seen in Fig. 10(b) taken from the experimental freezing sequence [23]. The droplet travels forward, while its tail is hooked to the frozen terrace left behind. Stabilization at an obtuse angle, which is possible only in 3D, makes unnecessary a hypothetic synchronization mechanism through heat exchange invoked in earlier 2D computations [24].

One could expect such an equilibrium configuration to be impossible during melting when the directions of motion of the phase transition front and the droplet slip given by Eq. (17) are opposite. This equation, however, is not applicable during melting transition, since, unlike freezing when the back part of the droplet sits on the terrace it has created, the droplet formed as a result of melting is attached to the high-energy side surface of the smectic layer on the melting edge, and is carried along as this edge propagates [7].

VI. CONCLUSION

The perturbation method described above is applicable to a variety of problems of droplet motion. It provides a practical way to resolve the contact line singularity and obtain quantitative relations applicable with a good precision under conditions of relatively slow motion when the droplet shape is only weakly distorted by viscous stresses. This analytical technique has allowed us, in particular, to elucidate the onset of motion (traveling bifurcation) that occurs, in analogy to activator-inhibitor systems, when diffusion and adsorption/desorption processes slow down, and to describe droplet interactions mediated by the surfactant depletion field.

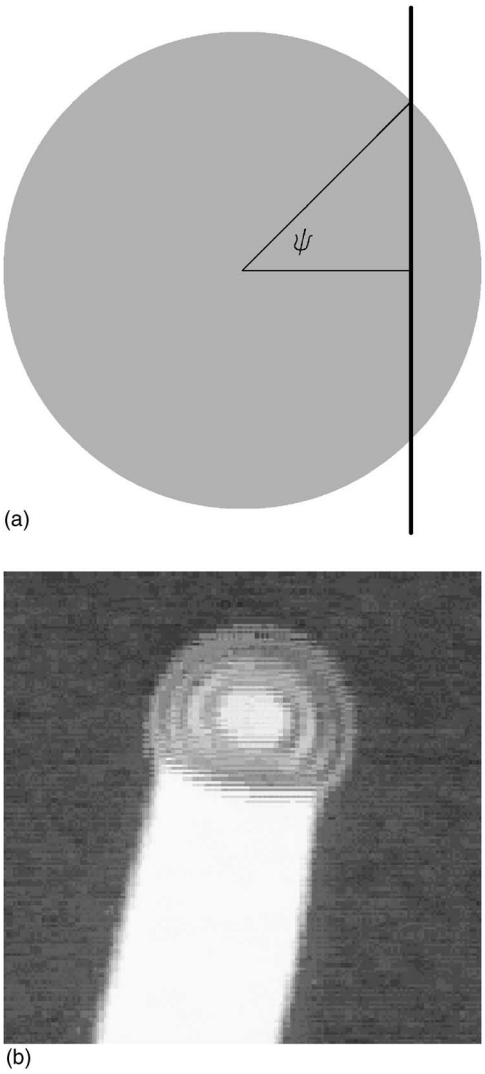

FIG. 10. (a) A droplet on a terrace. The smectic layer is thicker on the left of the terrace edge shown by the vertical line. (b) A snapshot from an experimental freezing sequence [23] showing a moving droplet leaving behind a frozen terrace (white and black areas correspond to thicker and thinner smectic layers, respectively).

ACKNOWLEDGMENTS

This work has been supported by Israeli Science Foundation (Grant No. 55/02). I acknowledge hospitality of MPIPKS (Dresden) and MPIKG (Golm) and thank Uwe Thiele for discussions of the theoretical model and Hans Riegler for discussions and access to his experimental data.

[1] C. D. Bain, G. D. Burnetthall, and R. R. Montgomerie, Nature (London) **372**, 414 (1994).
[2] F. Domingues Dos Santos and T. Ondarçuhu, Phys. Rev. Lett. **75**, 2972 (1995).
[3] S. W. Lee, D. Y. Kwok, and P. E. Laibinis, Phys. Rev. E **65**, 051602 (2002).
[4] D. W. Zheng, W. Wen, and K. N. Tu, Phys. Rev. E **57**, R3719 (1998).
[5] Y. Sumino, N. Magome, T. Hamada, and K. Yoshikawa, Phys. Rev. Lett. **94**, 068301 (2005).
[6] Y. Sumino, M. Nagayama, H. Kitahata, Shin-ichiro M. Nomura, N. Magome, Y. Mori, and K. Yoshikawa, Phys. Rev. E **72**, 041603 (2005).
[7] P. Lazar and H. Riegler, Phys. Rev. Lett. **95**, 136103 (2005).
[8] U. Thiele, K. John, and M. Bär, Phys. Rev. Lett. **93**, 027802 (2004).
[9] K. John, M. Bär, and U. Thiele, Eur. Phys. J. E **18**, 183 (2005).
[10] L. M. Pismen, Phys. Rev. Lett. **86**, 548 (2001).
[11] H. P. Greenspan, J. Fluid Mech. **84**, 125 (1978).
[12] F. Brochard, Langmuir **5**, 432 (1989).
[13] L. M. Hocking, Q. Appl. Math. **36**, 55 (1983).
[14] J. Eggers, Phys. Fluids **17**, 082106 (2005).
[15] L. M. Pismen and Y. Pomeau, Phys. Rev. E **62**, 2480 (2000).
[16] L. M. Pismen, Colloids Surf., A **206**, 11 (2002).
[17] L. M. Pismen and Y. Pomeau, Phys. Fluids **16**, 2604 (2004).
[18] L. M. Pismen and U. Thiele, Phys. Fluids **18**, 042104 (2006).
[19] K. B. Glasner and T. P. Witelski, Phys. Rev. E **67**, 016302 (2003).
[20] J. Eggers, Phys. Rev. E **72**, 061605 (2005).
[21] K. Krischer and A. Mikhailov, Phys. Rev. Lett. **73**, 3165 (1994).
[22] L. M. Pismen, *Patterns and Interfaces in Dissipative Dynamics* (Springer, Berlin, 2006).
[23] Video sequence, courtesy Hans Riegler.
[24] A. Yochelis and L. M. Pismen, Phys. Rev. E **72**, 025301(R) (2005).